GATING CURRENT HARMONICS

III. Dynamic Transients and Steaty States with Intact Sodium Inactivation Gating

JÜRGEN F. FOHLMEISTER*‡ AND WILLIAM J. ADELMAN, JR.*
*Laboratory of Biophysics, National Institute of Neurological and Communicative Disorders and Stroke, National Institutes of Health at the Marine Biological Laboratory, Woods Hole, Massachusetts 02543; and ‡Laboratory of Neurophysiology, University of Minnesota, Minneapolis, Minnesota 55455

ABSTRACT Internally perfused squid giant axons with intact sodium inactivation gating were prepared for gating current experiments. Gating current records were obtained in sinusoidally driven dynamic steady states and as dynamic transients as functions of the mean membrane potential and the frequency of the command sinusoid. Controls were obtained after internal protease treatment of the axons that fully removed inactivation. The nonlinear analysis consisted of determining and interpreting the harmonic content in the current records. The results indicate the presence of three kinetic processes, two of which are associated with activation gating (the so-called primary and secondary processes), and the third with inactivation gating. The dynamic steady state data show that inactivation gating does not contribute a component to the gating current, and has no direct voltage-dependence of its own. Rather, the inactivation kinetics appear to be coupled to the primary activation kinetics, and the coupling mechanism appears to be one of reciprocal steric hindrance between two molecular components. The mechanism allows the channel to become inactivated without first entering the conducting state, and will do so in about 40 percent of depolarizing voltage-clamp steps to 0 mV. The derived model kinetics further indicate that the conducting state may flicker between open and closed with the lifetime of either state being 10 μs. Dynamic transients generated by the model kinetics (i.e., the behavior of the harmonic components as a function of time after an instantaneous change in the mean membrane potential from a holding potential of -80 mV) match the experimental dynamic transients in all details. These transients have a duration of 7–10 ms (depending on the level of depolarization), and are the result of the developing inactivation following the discontinuous voltage change. A detailed hypothetical molecular model of the channel and gating machinery is presented.

INTRODUCTION

Two earlier papers (Fohlmeister and Adelman, 1985*a*, *b*) describe asymmetry (gating) currents in sinusoidally driven dynamic steady states for axons treated internally with protease sufficient to remove Na inactivation (Bezanilla and Armstrong, 1977). The results suggested two coupled processes in activation gating alone (the so-called primary, and secondary kinetics) that appear to operate with independent degrees-of-freedom. The secondary process contains two kinetic substates, one of which corresponds to the open activation gate. The primary process contains at least five kinetic substates where the relative occupation probabilities determine the likelihood of a transition to the open state. Here we give gating current records obtained from axons untreated with protease, with inactivation gating intact. These data were obtained both in dynamic steady states and as dynamic transients. The results indicate that the presence of inactivation selectively affects the primary process, leaving the secondary kinetics unchanged. This conclusion is based on direct inspection of the gating current records. The records show two outwardly directed current peaks at different phases during the sinusoidal period. The presence of inactivation gating reduces the peak that is associated with the primary activation kinetics, with no change in the secondary peak.

The fact that inactivation gating does not affect the gating current records during a substantial portion of the period strongly suggests that kinetic transition of inactivation gating do not contribute components to the gating current (Armstrong and Bezanilla, 1977). Because of the relatively large time constants associated with inactivation

Experiments were performed at the Marine Biological Laboratory in Woods Hole, MA. Computer simulations were supported in part by a grant from the University of Minnesota Academic Computing Services and Systems. J. F. F. was supported in part through research grant BNS-8415181 from the National Science Foundation. The authors acknowledge helpful conversations with Dr. Thomas L. Deits in connection with the protein biochemisty.

Send Correspondence to Dr. Jürgen Fohlmeister, Physiology Department, 6-255 Millard Hall, 435 Delaware Str. SE, University of Minnesota, Minneapolis, MN 55455.

gating, any direct gating current component would be observed otherwise throughout the sinusoidal period. The absence of such a component implies, in turn, that inactivation gating does not involve a charge movement in a direction normal to the plane of the membrane, and therefore cannot have a direct voltage-dependence of its own.

An attractive alternative proposes that the degree of inactivation present at a given time is determined by a mechanism of reciprocal steric hindrance between the inactivation and the primary activation mechanisms. This hypothetical mode of action finds support in the detailed harmonic analysis of the gating current records, for which the harmonic content shows characteristics of kinetic end-state saturation, which could be caused by a steric blockage of the primary activation mechanism due to the presence of inactivation. The full sodium channel gating mechanism thus involves three coupled processes, each with its own voltage-dependence for kinetic transitions, and its own weighting for contributions to the gating current. The primary activation kinetics operate with the strongest voltage dependence (Fohlmeister and Adelman, 1985*b*), the secondary kinetics have the largest weighting in generating gating current (Fohlmeister and Adelman, 1985*b*), and the inactivation kinetics operate with no direct voltage-dependence and zero weighting for gating current generation. The apparent discrepancy in the relative dominance of voltage-dependence and weighting between the primary and secondary activation processes is explained by the different dielectric media that transmit the gating current that is generated by the two processes. The molecular model of the sodium channel that is presented here (see Noda et al., 1984; Fohlmeister and Adelman, 1985*b*) gives the gating current component generated by the secondary kinetics as being transmitted through the aqueous portion of the channel, while the component generated by the primary kinetics is transmitted through protein or lipid. The differential dielectric constants of the two media are precisely what is needed to explain quantitatively the difference between voltage dependence and weighting of the two activation gating processes (Fohlmeister and Adelman, 1985*b*).

Although a harmonic analysis is prima facie a frequency domain analysis, we wish to point out that of the two independent variables of frequency, f, and mean membrane potential, E_{mean}, of the command sinusoid, frequency is of lesser importance in determining kinetic structure (Fohlmeister and Adelman, 1985*a*, appendix). This conclusion is based on the observation that the timbre (harmonic content) of the gating currents is a much stronger function of E_{mean} than it is of command frequency in both model simulations and axonal data. Quantitative changes in the timbre do occur as a function of the fundamental frequency, but it is the qualitative changes as a function of E_{mean} that are definitive for kinetic structure. The difference in the gating current generated by axons with intact inactivation gating and those without inactivation gating lies largely in the qualitative differences observed as functions of E_{mean}.

METHODS

Dynamic Steady State

Gating current records were obtained from squid (*Loligo pealei*) giant axons in sinusoidally driven dynamic steady states using voltage-clamp pulse profiles similar to those given by Fig. 1 in Fohlmeister and Adelman (1985*a*). The amplitude of the sinusoid was fixed at 35 mV (identical to that for the earlier paper). The mean membrane potential of the test sinusoid ($-110 \leq E_{mean} \leq +60$ mV), and the sinusosidal frequency ($0.5 \leq f \leq 4$ kHz) are the independent variables. The methods with regard to axon preparation, ionic solutions, and data acquisition and processing in dynamic steady states were the same as those given in Fohlmeister and Adelman (1985*a*), with the following changes: To obtain current records with the inactivation gating mechanism intact, an initial set of data was recorded before protease treatment of the axons. Data with inactivation gating removed were subsequently obtained after protease treatment of the same axons. The sinusoidal portion of both test and control pulses had a duration of 24 ms. Current records obtained during these 24-ms intervals were processed according to steps *a*, *c*, *d*, *f*, and *g* given in the Analysis of Current Records section in Fohlmeister and Adelman (1985*a*). Step *b* was changed to average 12 record pairs instead of the earlier four, to enhance the signal-to-noise ratio, because of the anticipated reduction in the gating current amplitude in the presence of inactivation (Armstrong and Bezanilla, 1977). Step *e* was changed to discard the first 12 ms of the averaged records, to allow for settling times into dynamic steady states. This increased settling time is due to the larger relaxation times associated with inactivation gating. The 12-ms settling time was established on the basis of the measured dynamic transients (see Figs. 5 and 8 herein).

Dynamic Transients

Dynamic transient data were derived from membrane currents that generated the command voltage profiles given in Fig. 1. The test voltage pulses consisted of a step from the holding potential of -80 mV to one of a set of mean membrane potentials, E_{mean}, in the range of -70 to 40 mV. The mean test potentials were spaced by 10 mV. The voltage sine wave

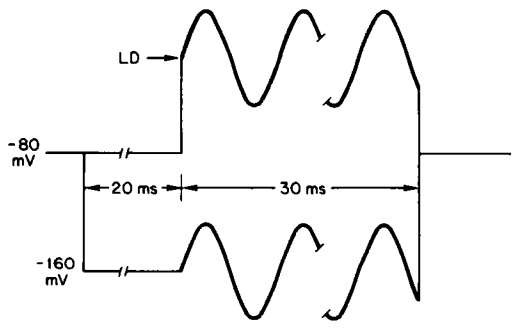

FIGURE 1 Command voltage-clamp pulse profiles for dynamic transient measurement. The two superimposed pulses in the figure constitute a test (*upper* trace) and control (*lower* trace) pulse pair (see text). The sinusoids in the test and control pulses have equal amplitude, frequency and phase. "LD" indicates the level of mean depolarization, E_{mean}, which, together with the sinusoidal frequency, constitute the two independent variables in this study.

generator (model FG 501; Tektronix Inc., Beaverton, OR) was triggered simultaneously with the step to E_{mean}, and its waveform was superimposed on E_{mean}. The sine wave amplitude was 35 mV (70 mV peak-to-peak) for all experimental (test and control) runs and in all model simulations.

Control records were obtained for a mean subtraction holding potential of −160 mV. Control pulses involved a step to −160 mV that was held for 20 ms before the onset of the superimposed sinusoid (see Fig. 1) to allow for settling time into a new steady state. Test and control pulses were generated in pairs. All pulses were spaced by 2 s. All current records were digitized by 5-μs intervals. To avoid a sampling artifact (see Fohlmeister and Adelman, 1985*a*, Synchronization and Stability section) the A/D converter and the sine wave generator were triggered by the same clock. After the computer acquisition of the digitized current records the data were reduced in the following series of steps by the laboratory computer (model PDP 11-60; Digital Equipment Corp., Maynard, MA): (*a*) The control record was subtracted from the test record point by point for each record pair. (*b*) The data from nine record pairs were averaged point by point to enhance the signal-to-noise ratio. (*c*) Segments of the data array from step *b* were extracted. The length of each segment was determined by, and equal to the period of the command sinusoid. That period was measured to the nearest 0.5 μs as described in Fohlmeister and Adelman, 1985*a*, the Analysis of Current Records section. The extracted segments were defined by the time of their onset measured relative to the test step to E_{mean} (or, equivalently, to the onset of the command sinusoid). The defining times were spaced by 100 μs, which led to substantial data record overlap among the segments. (*d*) The single period segments from step *c* were subjected to a fast Fourier transform (FFT) routine to extract the DC and fundamental components and the harmonic content as functions of the defining times. To take the FFT, the single period segments were sampled at 64 equally spaced points covering the period. To determine the 64 values, the computer was programmed to divide the externally supplied sine wave period by 64, and to pick off values from the data record segment at the resulting intervals. Because the 64 markers fell between two record points, in general, the 64 values required for FFT were determined by linear interpolation between the two flanking record points. For statements regarding the presence of noise in the data we refer to Fohlmeister and Adelman (1985*a*).

RESULTS

Current Records in Dynamic Steady States

Fig. 2 gives records of asymmetry (gating) currents obtained during sinusoidal voltage-changes of 35 mV amplitude about a series of mean membrane potentials, E_{mean}, in dynamic steady states. Records of the *left* panel were obtained from axons before internal protease treatment; those of the *right* panel were obtained after internal protease treatment sufficient to remove all apparent inactivation under square wave voltage-clamp. Of the two peaks per period that occur for certain values of E_{mean}, the first occurs during the rising phase, and the second during the falling phase of the command sine wave. It is apparent from this side-by-side comparison that differences between corresponding records in the two panels exist primarily in the relative magnitude of the first peak. For given E_{mean}, that peak is substantially increased after protease treatment, or, equivalently, for axons with no apparent inactivation under square-wave voltage-clamp.

Harmonic Analysis as a Function of E_{mean}

The bimodal distribution of gating current when elicited relative to a sinusoidal baseline (i.e., the control current records) implies the presence of a strong second harmonic component (Fohlmeister and Adelman, 1985*a*, *b*). Fig. 3 gives plots of the fundamental component and the second harmonic amplitudes in units of microAmperes per square centimeter as functions of E_{mean} for axons prior to protease treatment (solid curves) and after protease treatment

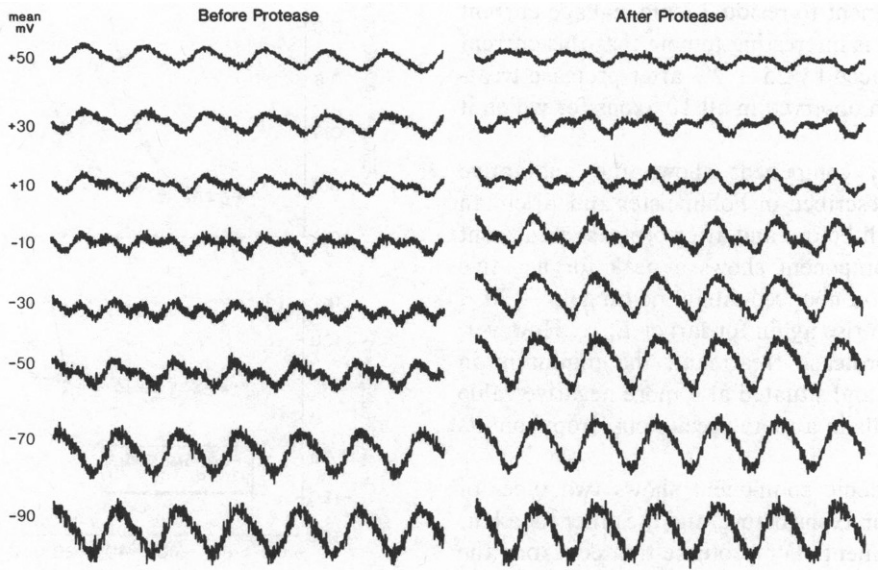

FIGURE 2 Gating current records obtained in dynamic steady states at f = 645 Hz for a series of values of E_{mean}. Records on the *left* were obtained before internal protease treatment of the axons, for which inactivation gating is intact. Records on the *right* were obtained after internal protease treatment sufficient to remove all apparent Na-inactivation. The peak associated with the primary activation kinetics may be identified from the records at large, negative E_{mean}, and followed as E_{mean} becomes more depolarized. The secondary kinetics correspond to the second peak that develops with increasing depolarization. See text for interpretation.

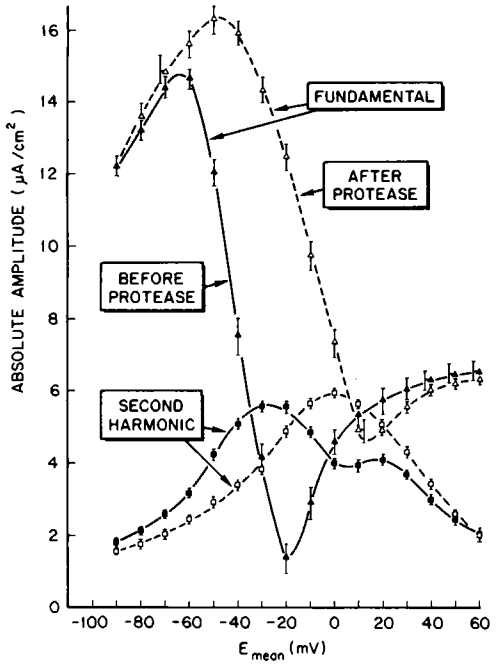

FIGURE 3 Absolute amplitudes of the fundamental component and the second harmonic contained in gating current records obtained in dynamic steady states, as functions of E_{mean}. Solid curves are for axons before protease treatment, and dashed curves are for axons after internal protease treatment. Data points correspond to the records given in Fig. 2. Error bars give one standard deviation among 10 experimental axons, with $550 \leq f \leq 700$ Hz.

(dashed curves). The DC component (not shown) is a linear function of E_{mean} with zero-current intercept equal to the mean subtraction holding potential, −160 mV. We attribute this component to residual ionic leakage current in the membrane. It is interesting to note that this current component was reduced by 25 ± 2% after protease treatment, a phenomenon observed in all 10 axons for which it was measured.

The fundamental component shows the qualitative behavior that was described in Fohlmeister and Adelman (1985*a*, Fig. 6). Both before and after protease treatment the fundamental component shows a peak for negative E_{mean}, followed by a pronounced dip in the range of $-20 < E_{mean} < +20$ mV, to rise again for larger E_{mean}. However, for axons before protease treatment, the minimum in amplitude is deeper and situated at a more negative value of E_{mean}, which results in a more precipitous drop from its peak value.

The second harmonic component shows two types of behavior, one type for axons before, and the other for axons after protease treatment. For protease-treated axons the second harmonic shows a single peak near $E_{mean} = 0$ mV. Untreated axons on the other hand, tend to produce a bimodal second harmonic curve with the larger peak occurring at $E_{mean} \cong -25$ mV, and a smaller peak at $E_{mean} \cong 15$ mV.

The third harmonic shows a broad and rounded peak near $E_{mean} = -35$ mV for both protease treated and untreated axons. This peak is correlated with a similar peak generated by a number of gating kinetic models, and is present because of the nonlinear voltage-dependence of the model rate constants, which generate surges in gating current near the extremes of the voltage range during the sinusoidal variation (Fohlmeister and Adelman, 1985*a*, appendix). In addition, axonal data obtained from untreated axons show a measurable third harmonic component for values of E_{mean} down to −60 mV, in contrast to protease treated axons. However, the third harmonic amplitude at its peak is only ~30% of the peak second harmonic amplitude. The amplitudes of the fourth and fifth harmonics can be comparable to the amplitude of the third harmonic for certain limited domains of E_{mean}, but are more typically at the noise level, as are all higher order harmonic amplitudes (see also Fohlmeister and Adelman, 1985*a*).

Fig. 4 *A* presents the second harmonic amplitude data in a normalized form such that the curve represents the ratio of the second harmonic to the fundamental component amplitude at each value of E_{mean}. Much of the data—both experimental and model simulation—were presented in

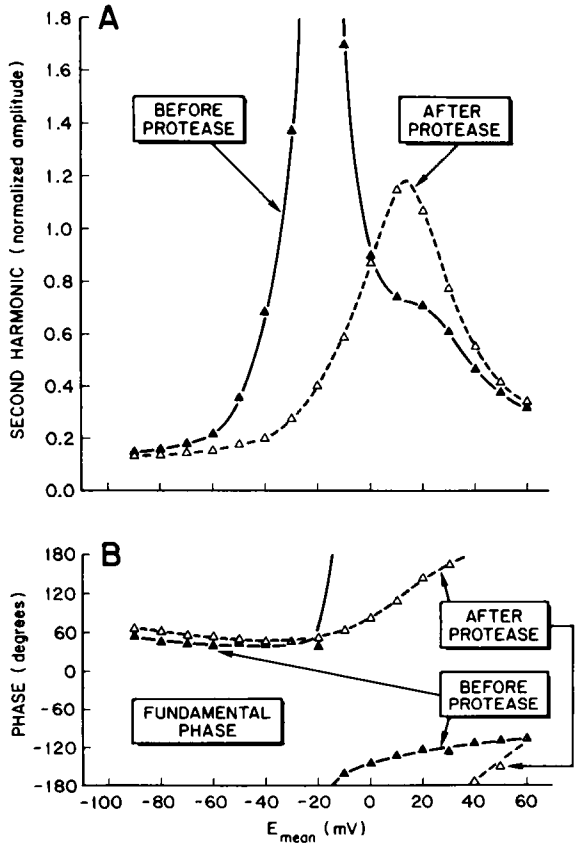

FIGURE 4 (*A*) Ratios of the amplitudes of the second harmonic to the fundamental component as functions of E_{mean} for the data given in Fig. 3. (*B*) Phases of the fundamental component as functions of E_{mean} for the data records in Fig. 2. Solid (dashed) curve is for data before (after) internal protease treatment of the axons, respectively.

this form in Fohlmeister and Adelman (1985*a*, *b*). Note that the second harmonic amplitude peak is shifted towards more negative values of E_{mean}, and that it assumes a much larger value and more pointed shape for untreated axons in comparison to that of protease treated axons. The relatively great size of this peak in the normalized amplitude was reproduced in every axon without exception, and reached value of 5 ± 2 for all frequencies of $0.5 \leq f \leq 4$ kHz. Also plotted in Fig. 4 *B* are the phases of the fundamental component as functions of E_{mean}. These phases exhibit the expected qualitative behavior for the series of records shown in Fig. 2 as explained in Fohlmeister and Adelman (1985*a*), the behavior being the relatively abrupt transition from positive values to negative values within the peak of the second harmonic amplitude. In addition, there appears to be a small reduction in the phase angles for E_{mean} on the negative side of the second harmonic peak for untreated axons as compared to protease treated axons.

The phase of the second harmonic (not shown) undergoes less variation as a function of E_{mean} for untreated axons in comparison to that of protease treated axons (see Fohlmeister and Adelman, 1985*a*, *b*), but otherwise has the same qualitative behavior.

Harmonic Analysis as a Function of Command Frequency

The data presented in Fig. 4 were obtained for a command (fundamental) frequency of $f = 645$ Hz. All of the qualitative features seen in that figure, as well as all of the discussion of the previous subsection holds for all frequencies in the experimental domain of $0.5 \leq f \leq 4$ kHz, for axons before protease treatment. The only observed quantitative effect is a narrowing, and a possible reduction in the peak of the normalized second harmonic amplitude centered at $E_{mean} = -19$ mV, for the higher command frequencies. The width of the peak at an amplitude of 1.4 is reduced by ~35% at 4 kHz as compared to that at 645 Hz. Beyond that, all phases are reduced in degree values as the frequency is increased, as previously described (Fohlmeister and Adelman, 1985*a*).

Dynamic Transients

Changes in the harmonic content due to the developing inactivation that follows depolarizing voltage steps from a holding potential of -80 mV were measured by employing the protocol given in Methods. For this set of data, the sine wave generator (35-mV amplitude) was triggered simultaneously with the voltage step to E_{mean} (see Fig. 1). Segments of the resulting gating current records of precisely one period of the command sinusoid in length were extracted with the starting point of consecutive segments advanced in time by 100 μs. (Given the 100-μs shift from segment to segment implies a good deal of data record overlap from one segment to the next at the experimental command frequencies.) These segments were each subjected to Fourier analysis. The resulting harmonic contents are (computer) plotted in Fig. 5 as functions of the time interval between the clamp step to E_{mean} and the beginning of the analyzed record segment. Note that the greatest changes in the harmonic content during the transient occur in the fundamental component for $-50 \leq E_{mean} \leq 0$ mV. Less pronounced changes occur in the second harmonic component. These results are consistent with the dynamic steady state data when one associates the initial ($t = 0$) values of the transients with steady state data for axons after protease treatment, and further associates the asymptotic values of the transients with steady state data for axons before protease treatment (see Fig. 2). Note that the dynamic transients are within $1/e$ of their final (steady state) value after 3–5 ms, and are fully over at 7–10 ms, depending on E_{mean}. The transients are therefore clearly not of an exponential form. These transients did not appear for protease treated axons, and the corresponding curves were flat for times beyond the first 2 ms.

The dynamic transients data exhibit rapid fluctuations during the first 2 ms. The immediate and consistent interpretation of those fluctuations is that they are due to the activation gating kinetics settling into a (near) dynamic steady state for the new value of E_{mean} (see Fohlmeister and Adelman, 1985*a*, the Analysis of Current Records section, point *e*). Because the model proposed in the following subsection gives a coupling between the activation and

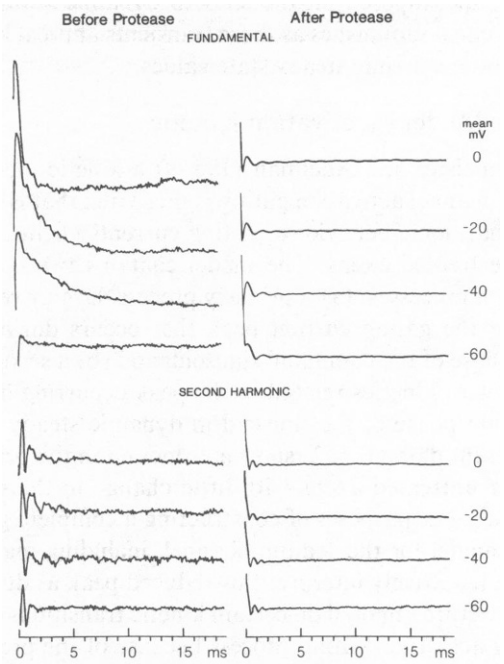

FIGURE 5 Fundamental component and second harmonic as functions of time contained in gating current records during the dynamic transient that follows the voltage-clamp step from -80 mV to E_{mean} for a series of values of E_{mean}. *Left* (*right*) panels are for dynamic transients obtained before (after) internal protease treatment, respectively. $f = 738$ Hz. See text for interpretation.

inactivation gating kinetics, the activation kinetics cannot reach a true dynamic steady state until the inactivation kinetics have also settled at the new value of E_{mean}. However, the activation gating portion of the kinetics will be near the dynamic steady state for the degree of inactivation present at each point throughout the transient (except the first 2 ms), because the time constants for changes in inactivation are relatively large compared to the command sine wave period.

A further feature evident throughout the dynamic transient is a periodic wave-form, with the period of the command sinusoid, superimposed on the smooth transition. Unlike record segments obtained in dynamic steady state, for which the beginning and ending values are equal by definition, each Fourier-analyzed record segment of the dynamic transient begins and ends with a slightly different value. Furthermore, the difference between the beginning and ending values will vary from segment to segment, and can also change sign. This is because consecutive segments occur at different phases of the command sinusoid, the phase difference being (100 μs/sin wave period)360°, and the gating current is a rapidly changing function throughout the period. The nonzero difference between the beginning and ending values of the function is equivalent to a discontinuity for purposes of Fourier analysis. Although most of the discontinuity will contribute to harmonic components of higher order, its presence will nonetheless also affect the low order harmonics and the fundamental component. This is the cause of the periodic wave-form that is superimposed on the smooth dynamic transients, and the effect diminishes as those transients approach their asymptotic, dynamic steady state values.

Model Inactivation Kinetics

In Fohlmeister and Adelman (1985*b*) a kinetic model of sodium channel activation gating is presented that is based on the harmonic behavior of gating currents elicited from protease treated axons. The model contains two coupled transition processes: (a) a primary process, largely responsible for the gating current peak that occurs during the rising phase of the command sinusoid; and (b) a secondary process with kinetics related to the peak occurring during the falling phase of the sinusoid in dynamic steady state. The present data (Fig. 2) show a reduction in the primary peak for untreated axons with little change in the secondary peak. For purposes of constructing a complete gating kinetic model for the sodium channel, including inactivation, we tentatively interpret this reduced peak as due to a steric stricture imposed on certain kinetic transitions of the primary activation gating process because of the presence of inactivation (see Discussion). Further, because the secondary kinetics appear to be unaffected, and because those secondary kinetics respond specifically to the transition $x_4 \rightleftarrows x_5$ of the primary kinetics (see Fohlmeister and Adelman, 1985*b*), that steric stricture is tentatively interpreted as affecting transitions to, and among states x_3, x_2, and x_1 of the primary kinetics (Fohlmeister and Adelman, 1985*b*). Thus, the primary kinetic equations are amended to read

$$\dot{x}_1 = -k_{12}x_1 + k_{21}x_2 \tag{1a}$$

$$\dot{x}_2 = -(k_{21} + k_{23})x_2 + k_{12}x_1 + k_{32}x_3 \tag{1b}$$

$$\dot{x}_3 = -(k_{32} + k_{34})x_3 + k_{23}x_2 + k_{43}hx_4 \tag{1c}$$

$$\dot{x}_4 = -(k_{43}h + k_{45})x_4 + k_{34}x_3 + k_{54}x_5 \tag{1d}$$

$$\dot{x}_5 = -k_{54}x_5 + k_{45}x_4, \tag{1e}$$

where the inactivation state variable, h, has the same functional interpretation as the Hodgkin-Huxley (1952) model state variable h, but whose variations are generated by an entirely different mechanism (see below).

Eqs. 1a–e are written in terms of the probability that a channel is inactivated. This form is appropriate in the analysis of gating current data that describes the behavior of a population of channels. Equations for single channel kinetics—where inactivation is all or none—follow directly from the kinetic diagram given in Fig. 9 (see Discussion).

Note that only Eqs. 1c and 1d differ from the corresponding set of Eqs. 1a–e in Fohlmeister and Adelman (1985*b*). The difference is a simple replacement in only one rate constant

$$k_{43} \rightarrow k_{43}h. \tag{2}$$

This replacement reflects the proposed requirement that the transition rate from state x_4 to lower states is proportional to the probability that the channels are not inactivated, and that transition rate becomes zero when the channels are inactivated ($h = 0$). Therefore, the mass kinetic equations are consistent with the hypothesis that states x_1, x_2, and x_3 become inaccessible for the fraction of channels that are inactivated, allowing only transitions between states x_4 and x_5 of the primary activation kinetics in that case. Further justification for placing the cutoff point of accessible states at x_4 is given in the Appendix.

For the inactivation process itself, we propose the following two-state kinetic equation

$$\dot{h} = -K_{01}h\frac{x_4 + x_5}{x_1 + x_2 + x_3 + x_4 + x_5} + K_{10}(1 - h), \tag{3}$$

where the variables x_i ($i = 1, \ldots, 5$) are the dimensionless population probabilities for states of the primary activation gating kinetics. This equation describes the development of the inactivated state as the result of shifting populations to higher index substates of the primary activation kinetics. Therefore, the degree of inactivation in a population of channels depends specifically on the relative magnitudes of the two sums $(x_4 + x_5)$ and $(x_1 + x_2 + x_3)$. (Note that the rate of removal of inactivation is independent of the

primary activation gating process.) One mechanistic interpretation that is consistent with this mass kinetic equation is that inactivation cannot develop in channels whose primary activation process occupies states x_1, x_2, or x_3 again because of steric hindrance. Therefore, in this interpretation a portion of the sodium channel gating operates by reciprocal steric constraints imposed by inactivation onto the primary kinetics, and in turn by the primary mechanism onto the inactivation transitions; inactivation cannot develop in a channel in state x_1, x_2, or x_3, and an inactivated channel cannot enter those same states. Inactivation, therefore, derives its voltage dependence indirectly from the primary activation process and has no direct voltage dependence of its own (see Discussion for further justification of this condition). The rate constants

$$K_{01} = 2.0 \text{ ms}^{-1} \tag{4a}$$

and

$$K_{10} = 0.125 \text{ ms}^{-1} \tag{4b}$$

were adjusted to fit the harmonic data (see below), and are consistent with the rates of development and removal of inactivation measured in sodium-ionic current under voltage-clamp (Hodgkin and Huxley, 1952). With the usual normalization for probabilities

$$\sum_{i=1}^{5} x_i = 1.0 \tag{5}$$

Eq. 3 may be rewritten in the form

$$\dot{h} = -K_{01}h(x_4 + x_5) + K_{10}(1 - h). \tag{6}$$

For completeness we also reproduce here the unaffected and unaltered secondary kinetic Eqs. 1f and g of Fohlmeister and Adelman (1985*b*)

$$\dot{x}_0 = -\kappa_{06}(x_1 + x_2 + x_3 + x_4)x_0 + \kappa_{60}x_5x_6 \tag{1f}$$

$$\dot{x}_6 = -\kappa_{60}x_5x_6 + \kappa_{06}(x_1 + x_2 + x_3 + x_4)x_0. \tag{1g}$$

Values and voltage-dependences of the rate constants of the primary and secondary activation kinetics are given in Eqs. 5a–h, 6a and b, and 7a and b in Fohlmeister and Adelman (1985*b*).

Harmonic Analysis of Model Gating Current

Fig. 6 gives the fundamental and second harmonic amplitudes as functions of E_{mean} of the model-simulated gating currents in dynamic steady states for $f = 500$ Hz. Gating current, i_g, is given by the expression

$$i_g(t) = 6[k_{12}x_1 + (k_{23} - k_{21})x_2 + (k_{34} - k_{32})x_3 + (k_{45} - k_{43}h)x_4 - k_{54}x_5 + 2(k_{06}x_0 - k_{60}x_6)], \tag{7}$$

where k_{06} and k_{60} are defined by Eqs. 2a and b of

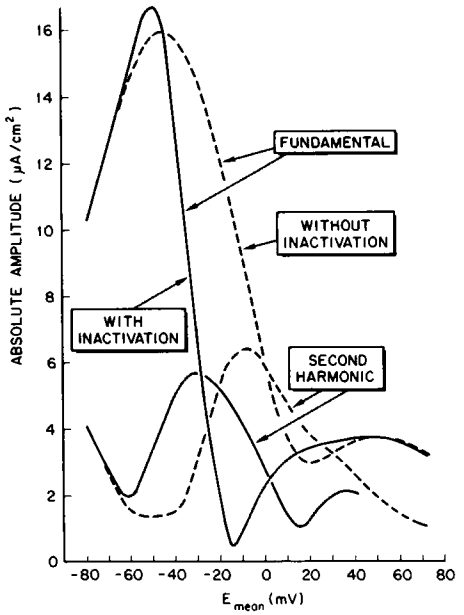

FIGURE 6 Amplitudes of the fundamental component and second harmonic contained in simulated, model-generated gating current records in dynamic steady states at $f = 500$ Hz as functions of E_{mean}. Solid curves are for the full model including inactivation gating, and dashed curves are for the model with $h = 1$. See text for details.

Fohlmeister and Adelman (1985*b*). The dashed curves of Fig. 6 give the amplitudes of the fundamental and second harmonic for the model with inactivation removed ($h = 1$). This figure may be compared directly with Fig. 3, which gives the corresponding experimental data. Fig. 7 gives the model data for the normalized second harmonic amplitude (that is, the ratio of the second harmonic to the fundamental component for each value of E_{mean}), as well as the phase data for the fundamental component.

Fig. 8 gives dynamic transients for model generated gating currents for $E_{mean} = -35$ mV and $f = 500$ Hz. To obtain these model data, the kinetic equations were integrated using initial values of the state variables x_i and h equal to their steady state values at $E = -80$ mV. The curves may therefore be compared directly with the corresponding experimental dynamic transients given in Fig. 5. Note the close correspondence between the theoretical and experimental curves in all details discussed in the Dynamic Transients section. This correspondence holds for all values of E_{mean}.

DISCUSSION

The full sodium channel gating kinetics given in Results contain three coupled processes: The primary activation process (identified by its molecular substates x_i, where $i=1$, 2, 3, 4, or 5), the secondary activation gating process (identified by its molecular substates x_j, where $j=0$ or 6), and the inactivation gating process described by the state variable h. To place inactivation on a uniform mathemati-

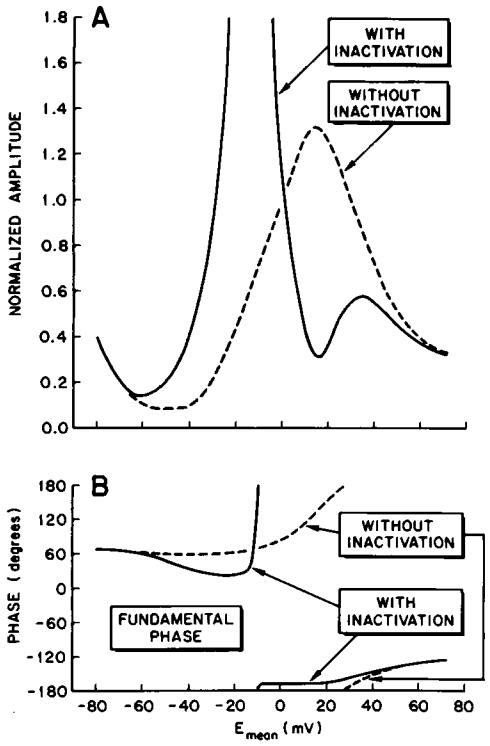

FIGURE 7 (*A*) Ratios of the amplitudes of the second harmonic to the fundamental component as functions of E_{mean} for the model-generated data given in Fig. 6. (*B*) Phases of the fundamental component in model-simulated gating current records corresponding to the simulations given in Fig. 6. Solid curves are for the full model including inactivation gating, and dashed curves are for the model with $h = 1$.

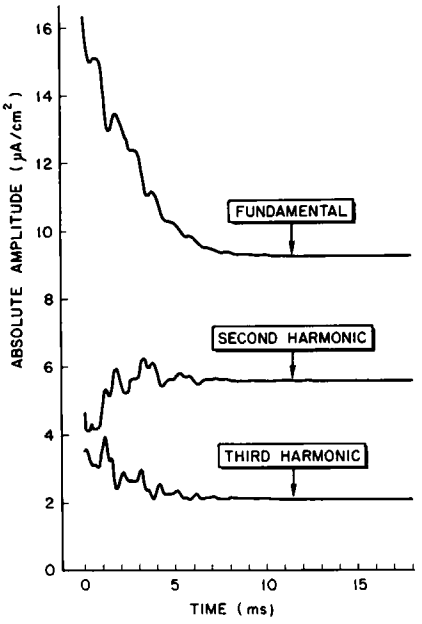

FIGURE 8 Model-generated harmonic amplitudes during dynamic transients at $E_{mean} = -35$ mV and for $f = 500$ Hz. Model gating currents were generated by integrating the kinetic equations using a Runge-Kutta routine on a Cyber 845 computer (Control Data Corp., Minneapolis MN). 2-ms segments of the simulated current records were subjected to an FFT routine on the basis of 16 equally spaced record samples. Successive segments were obtained by advancing the segment onset times by 2 ms/16 = 125 μs. The curves in the figure connect the resulting data points spaced by 125 μs.

cal basis with the activation equations given in Fohlmeister and Adelman (1985*b*), Eqs. 3 or 6 may be replaced by the overdetermined set

$$\dot{h}_0 = -K_{01}h_0(x_4 + x_5) + K_{10}h_1 \quad (8a)$$

$$\dot{h}_1 = -K_{10}h_1 + K_{01}h_0(x_4 + x_5), \quad (8b)$$

where

$$h_0 + h_1 = 1. \quad (8c)$$

In this form the two substates h_0 and h_1 play roles analogous to those of the x_i for activation gating, with h_1 equal to the probability that a channel is, and h_0 equal to the probability that a channel is not inactivated. For consistency in notation with Fohlmeister and Adelman (1985*b*, Fig. 6), the symbol for overall molecular conformation $X_{i,j,l}$, must then carry three noncommutative indices, where the third index, $l = 0$ or 1, identifies the substate of the inactivation process.

Fig. 9 gives a complete kinetic diagram for the model of sodium channel gating for which primary activation, and inactivation gating are sterically constrained. The lower level of this diagram is identical to the kinetic diagram for activation gating given in figure 6 of Fohlmeister and Adelman (1985*b*). In this figure the seven conformations corresponding to states on the *left* half of the diagram (that is, states with second index 0) have open activation gates (see Fohlmeister and Adelman, 1985*b*). The remaining seven conformations, on the *right* half of the diagram (states with second index 6) correspond to closed activation gates. The four conformations $X_{i,j,1}$ of the *upper* level in the diagram are all inactivated conformations, and therefore

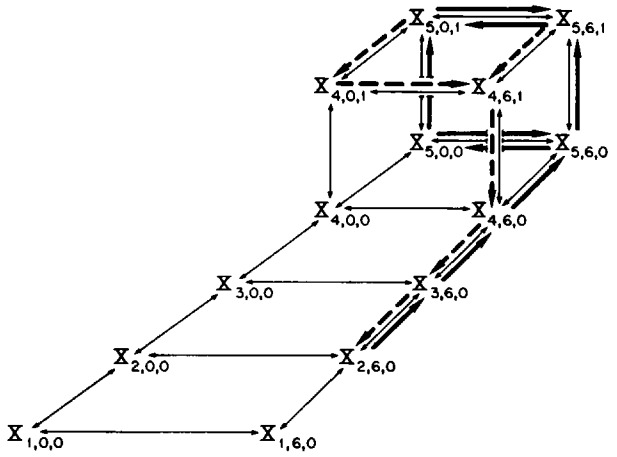

FIGURE 9 Kinetic diagram for the model sodium channel. Heavy arrows indicate the most common kinetic transitions after a moderate to large depolarization (solid) and after repolarization (dashed). See text for details.

nonconducting. The lower ten conformations, $X_{i,j,0}$, correspond to non-inactivated channels.

Rate constants for transitions that change the first index of conformations X, are of the primary activation kinetics and are strongly voltage-dependent (see Fohlmeister and Adelman, 1985*b*, Eqs. 6a and b). Rate constants for transitions that change the second index, $0 \rightleftarrows 6$, are of the secondary activation kinetics and are weakly voltage-dependent. Vertical transitions between $X_{i,j,1}$ and $X_{i,j,0}$ produce (upward), or remove (downward) inactivation and are not voltage-dependent.

Given the values of the rate constants, the dominantly populated state in steady state at -60 mV is $X_{2,6,0}$ (c.f. Fohlmeister and Adelman, 1985*b*). The most commonly occurring conducting state is $X_{5,0,0}$ (Fohlmeister and Adelman, 1985*b*). Conformation $X_{4,0,0}$ will occur rarely, and $X_{i,0,0}$ (i=1, 2, 3) almost never, although they are not sterically restricted in any way. Given certain assumptions about the behavior of single channel molecules (see Fohlmeister and Adelman, 1985*b*, Discussion) the molecule will undergo rapid fluctuations between $X_{5,0,1}$ and $X_{5,6,1}$ (lifetimes ~10 μs) in steady state at any moderate to large ($\gtrsim -30$ mV) depolarization. Those rapid transitions will occur between conformations $X_{5,0,0}$ and $X_{5,6,0}$ during the first millisecond or two after the depolarizing voltage step, and can account for any conducting state flicker seen in single channel recordings of sufficient temporal resolution (Fohlmeister and Adelman, 1985*b*). Also shown in Fig. 9 are the most common kinetic paths after a depolarization from -60 mV (heavy solid *arrows*) and after a repolarization to -60 mV (heavy dashed *arrows*). These kinetic paths can be compared to the most common kinetic paths in the absence of inactivation shown in Fig. 6 of Fohlmeister and Adelman, (1985*b*) by projecting the present kinetic diagram onto a horizontal plane.

Although most common, the transition $X_{4,6,0} \rightarrow X_{5,6,0}$ will often be replaced by $X_{4,6,0} \rightarrow X_{4,6,1} \rightarrow X_{5,6,1}$, which leads to inactivation without prior conduction. The latter transitions will occur in 38% of channels for a depolarization to 0 mV [$K_{01}/(k_{45} + K_{01}) = 0.38$]. This percentage will vary with the level of depolarization in accordance with the voltage-dependence of the rate constant k_{45}.

The proposed reciprocal steric hindrance mechanism is based solely on our interpretation of the harmonic behavior of the gating currents: The amplitude of the second harmonic increases as E_{mean} is reduced from 0 mV, followed by a relatively precipitous falloff near $E_{mean} = -50$ mV. Further, the amplitude of the third harmonic remains substantial in the same range (see Results). From the limited set of nonlinear mechanisms found in model simulations of gating kinetics (Fohlmeister and Adelman, 1985*a*, *b*), this behavior was immediately suggestive of an end-state saturation phenomenon, and that saturation effect is relieved at the more negative values of $-60 \lesssim E_{mean} \lesssim -40$ mV. The simplest way to induce such end-state saturation in an otherwise non-saturating kinetic scheme is to cause a steric blockade in that scheme, thereby preventing kinetic transitions to states further down the line. That blockade is naturally interpreted as being due to inactivation because of the occurrence of the non-linear phenomenon only in channels with an intact inactivation mechanism (i.e., in membranes untreated with protease), and because the harmonics characteristic of end-state saturation vanish at values of $E_{mean} \lesssim -50$ mV, for which the majority of channels is no longer inactivated. If the harmonic data are to be interpreted in this way, then it is necessary to assume that transitions in the inactivation process itself should contribute little or nothing to the gating current (see also Armstrong and Gilly, 1979), because such a current component would affect the harmonic behavior. Therefore, voltage is ruled out as the principal motive force for changes in the state of inactivation, leaving reciprocal steric blockade as an attractive alternative; the theory is then internally consistent.

The hypothesis of reciprocal steric blockade is consistent with gating current data obtained under square wave voltage clamp. In that case the OFF response (response after the repolarizing voltage-step of a square-wave $P/4$ protocol) declines in peak magnitude with the time course of developing inactivation as the repolarizing step is increasingly delayed relative to the depolarizing (ON response) step (Armstrong and Bezanilla, 1977). The asymptotic OFF response peak is roughly 1/3 of the peak value of the ON response (Armstrong and Bezanilla, 1977). The present kinetics closely mimic these data. However, this model suggests a point of complexity that is not readily apparent in the transient data alone: Because of the presence of two coupled activation gating processes with independent voltage-dependences, oscillatory responses become possible during ON and OFF transients. However, for square-wave voltage pulses, no oscillation is predicted during the OFF transient, and that transient follows the solid curve given in Fig. 10. Nevertheless, the OFF transient is on the verge of oscillating (Fig. 10, dashed

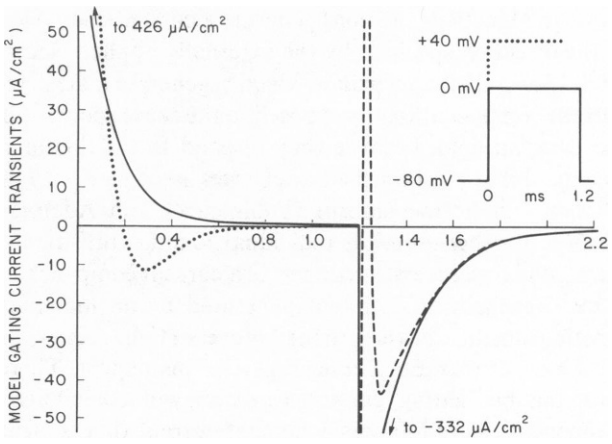

FIGURE 10 Model-generated gating currents in response to the simulated square wave voltage clamp pulses given in the *inset*. See test for interpretation.

curve), but is prevented from doing so by the weak voltage-dependence of the secondary process rate constants for the high-frequency Fourier components that constitute the voltage waveform in the immediate vicinity of the step. This point is amplified in the Appendix.

On the other hand, the transient of the ON response contains a model gating current component due to the secondary kinetics that involves only lower frequency Fourier components of the voltage-waveform. The difference occurs because the secondary kinetics come into play only after a time delay during which the primary kinetics are shifting populations from low index substates to substates x_4 and x_5 in preparation for secondary kinetic transitions. Using the voltage-dependence of the secondary process rate constants derived for $f = 500$ Hz, the model ON transient shows a current reversal after a large, instantaneous (no rising phase) outwardly directed gating current, provided that the depolarization is to $> +10$ mV. Fig. 10 (dotted curve) gives the predicted ON transient for a depolarization to $+40$ mV; the corresponding OFF response (not shown) contains only those features already discussed above. The current reversal within the ON response is perhaps the most definitive model prediction for gating current transients. Unfortunately, the reversed current magnitude is small in comparison with that of the initial current peak, and is therefore subject to masking by a possible gating current component due to K-channel gating (Gilly and Armstrong, 1980; Bezanilla et al., 1982). Nevertheless, this phenomenon may have already been observed in a different form in frequency domain studies based on random fluctuations (Fishman et al., 1977; Takashima, 1978; Taylor and Bezanilla, 1979). Those papers present and discuss the observation that the membrane capacitance appears to decline somewhat when the dielectric current is measured at more depolarized potentials. This observation was puzzling, because the presence of a gating current component in the dielectric current was expected to increase the measured membrane capacitance. This expectation was based on the implicit assumption that all gating kinetic transitions generate a current component in the direction specified by the externally applied electric field. However, the secondary kinetics generate a dielectric current component that is opposed to the sense specified by the external field, because they respond to the dominant local field that is established by charges associated with the primary kinetic mechanism (Fohlmeister and Adelman, 1985*b*). Furthermore, an individual kinetic transition of the secondary process will generate a current component of twice the magnitude of that generated by an individual kinetic transition of the primary process (Fohlmeister and Adelman, 1985*b*; Eq. 8, and Eq. 7 in this paper). Therefore, the net gating current can and will contribute a component to the total displacement current that is of the opposite sign from that of the nonspecific capacitative current, but only when that current is measured at membrane potentials for which x_4 and x_5 are the dominantly populated substates of the primary activation kinetics (i.e., for moderate and large depolarizations).[1] The strongly voltage-dependent transitions $x_4 \rightleftarrows x_5$ then induce the transitions $x_0 \rightleftarrows x_6$ of the secondary kinetics, with the secondary transitions contributing the larger component to the gating current. This "peculiar" effect is possible provided that the current paths across the membrane have widely different dielectric constants for the two processes, with the path of the secondary process being water (the aqueous channel itself), and that of the primary process being protein and lipid (see Fohlmeister and Adelman, 1985*b*, Discussion).

Although a given single channel is either fully inactivated (in substate h_1) and nonconducting or not inactivated (in substate h_0), a population of sodium channels will not fully inactivate in steady state at any membrane potential. Specifically, $h_\infty(E) \rightarrow 0.059$ asymptotically for large depolarizations ($E \rightarrow \infty$). This asymptotic value is a direct result of the kinetic Eq. 6 in conjunction with the rate constants given in Eq. 5. On the other hand, inactivation is fully removed in the population for large hyperpolarizations: $h_\infty(E) \rightarrow 1$ as $E \rightarrow -\infty$ (see Fig. 11 *A*). Although this behavior is somewhat different from that given by the Hodgkin-Huxley model (for which $h_\infty(E) \rightarrow 0$ as $E \rightarrow \infty$), we feel that the difference does not warrant a revision of the present kinetics because of the indirect way in which the Hodgkin-Huxley variable h was determined, and the associated inherent uncertainties and errors. Fig. 11 *B* gives Na-ionic currents generated by the present model under square wave voltage-clamp, that clearly show the incomplete inactivation. Although one might expect substantial Na-tail currents under this condition, in fact, tail currents are insignificant and short-lived. In addition, inactivation as presented herein offers a better behaved membrane potential trajectory immediately after action potentials (Fig. 11 *C*) as compared to that of the Hodgkin-Huxley model; the present model gives a less squared-off transition from the falling phase of the action potential to the post-impulse undershoot. The initial trajectory and threshold behavior of action potentials generated in response to anode-break excitation (not shown) are also well behaved. A molecular gating mechanism consistent with these kinetics is given in the Appendix.

APPENDIX

Properties of the Kinetics

The symbol $X_{i,j,l}$ was introduced in the Discussion as an identifier of molecular conformations, such that for a given single channel molecule

[1] Asymmetry current for $E_{mean} \geq 40$ mV may be contaminated by Cl^- and Cs^+ leakage current. When E_{mean} is increased above $+40$ mV, the DC component derived from Fourier analysis begins to depart from strict linearity as a function of E_{mean}, and an outwardly directed current peak develops that is in phase with the command sinusoid. These are the signatures of voltage-dependent leakage conductance, and they are absent for $E_{mean} < +40$ mV. The sinusoidal component of a linear leakage current component is automatically subtracted in data reduction.

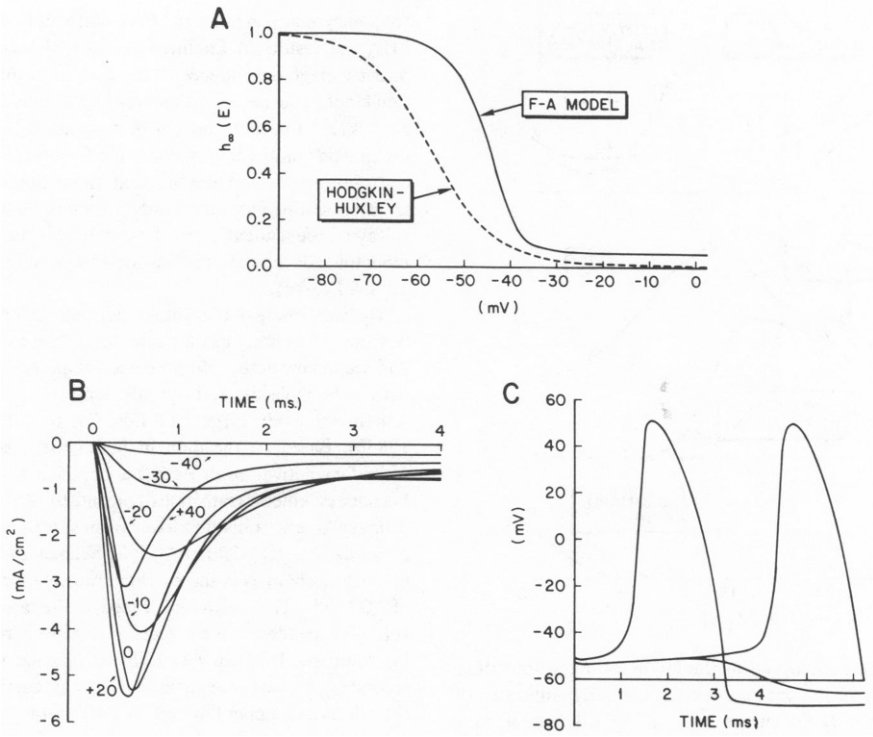

FIGURE 11 (*A*) Steady state values of inactivation, h_∞, as functions of the membrane potential, E, for the present kinetic model (solid curve) and for the Hodgkin-Huxley model (dashed curve). The curves represent the probability, or fraction of channels not inactivated in steady state at a given voltage. (*B*) Sodium-ionic currents generated by the present kinetic model following depolarizing voltage-clamp steps from a holding potential of −60 mV to the test potentials that identify individual curves. $\bar{g}_{Na} = 650$ mS/cm² (see Fohlmeister and Adelman, 1985b). Note the incomplete inactivation. (*C*) Action potentials and a subthreshold response generated by the present kinetic model after an instantaneous depolarizing current shock from the resting potential (−60 mV) to −51, −52.88, and −52.9 mV. To generate these responses the present sodium channel gating kinetics were supplemented with K-channel gating kinetics given by the Hodgkin-Huxley model for 8°C. $\bar{g}_K = 60$ mS/cm² in conjunction with $\bar{g}_{Na} = 650$ mS/cm².

each of the three indices has a specific value at any instant of time, subject to the constraint that $l = 1$ cannot occur in conjunction with $i = 1, 2$, or 3. This constraint reflects the reciprocal steric blockade between the primary activation kinetics and the inactivation kinetics. In addition to its role of identifying molecular conformations, $X_{i,j,l}$ can also be given a value (a number between zero and one) equal to the probability, or fraction of channels in each particular conformational state. When that probability is computed from the mass kinetic equations, its value is given by the product,

$$X_{i,j,l} \equiv x_i x_j h_l, \tag{A1}$$

of the probabilities of the individual substates of the three gating kinetic processes, and therefore automatically satifies the normalization condition

$$\sum_{i=1}^{5} \sum_{j=0,6} \sum_{l=0}^{1} X_{i,j,l} = 1. \tag{A2}$$

Note that Eq. A1 leads to nonzero probabilities for the "forbidden conformations" $X_{1,j,1}$, $X_{2,j,1}$, and $X_{3,j,1}$. Evidently, the mass kinetic equations alone do not contain within them the specific requirement of a reciprocal steric blockade, even though they were written with that assumption in mind. The reason is that the replacement of k_{43} by $k_{43}h$ (Eq. 2) describes the mass effect, but not the cause, of the reduced transition rate $x_4 \rightarrow x_3$ in a population of channels with a certain fraction, $1 - h = h_1$, of the channels inactivated, but a one-to-one relationship between the mass kinetic equations and a model mechanism does not exist. Indeed, the given kinetic equations are less specific than the kinetic diagram (Fig. 9), and could have either a probabilistic or a deterministic interpretation of the effect of inactivation at the single channel level. If one assumes a mechanism of reciprocal steric hindrance, then the interpretation must be specifically deterministic because the applicable (classical) physical laws prevent two molecular components from occupying the same space at the same time, and this is reflected in the kinetic diagram. In the case of the coupling of the secondary activation to the primary activation kinetics we faced a similar choice of interpretation, and there resolved it in favor of a probabilistic interpretation (see Fohlmeister and Adelman, 1985*b*, Discussion).

Given the reciprocal steric hindrance hypothesis, the cutoff for accessible states in the primary activation process for inactivated channels must be placed at x_4. This follows because simulations with that cutoff state closely match the harmonic data, whereas simulations with the cutoff at x_3 or lower states resulted in harmonic behavior that has some qualitative similarities, but has no quantitative correspondence to that of the data. Fig. 12 shows the effect of the blockade due to inactivation on the temporal behavior of state variables x_3 and x_4 in dynamic steady state at $E_{mss} = -32$ mV. Note the large accumulation of channels in substate x_4, and the depletion of channels in substate x_3, during the falling phase of the command sinusoid, that is, the phase during which the voltage dependence of the primary process rate constants is such as to tend to reduce the index value of its substates.

The kinetics (Fig. 9) satisfy detailed dynamic balance because all primary activation rates that transit from conformations with the same first index to new conformations with the same first index are equal for any fixed voltage. Further, all horizontal (secondary activation process) transition rates pointing in one direction (either left or right) are equal for any fixed voltage once the primary process has settled into its steady state distribution of states at that voltage. Finally, all vertical transition rates

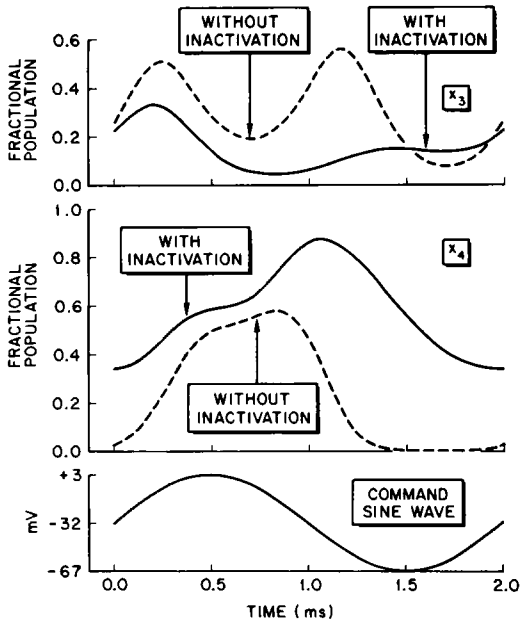

FIGURE 12 Time-varying populations of the model primary activation kinetic substates x_3 and x_4 during one sinusoidal cycle in dynamic steady state at $E_{mean} = -32$ mV. Solid curves are for the full model with inactivation gating, and dashed curves are for the model with $h = 1$. See text for interpretation

pointing in one direction (either up or down) are equal, again once the primary process is situated in a steady state distribution (c.f. Eq. 6). Therefore, net circulation in any closed kinetic loop is precluded in steady state at any fixed membrane potential.

Secondary Activation Kinetics, Near Oscillatory Response

Fig. 10, dashed curve, gives an OFF gating current transient generated by the model with parameters appropriate to dynamic steady state data for $500 \leq f \leq 700$ Hz. Uncorrected for the high frequency components inherent in a step function, the model predicts large amplitude fluctuations during the initial ~50 μs of the OFF response. The fluctuation begins with an instantaneous (no rising phase), negative (inwardly directed) current of about -2 mA/cm^2. This current begins an immediate decline, crosses zero at ~12 μs, overshoots to a positive current peak of ~450 μA/cm^2 at ~25 μs, only to reverse its direction (sign) again at ~45 μs, to reach a second inwardly directed peak at ~100 μs. (All times are relative to the OFF voltage-step.) The model current then declines without further oscillation to an asymptotic value of zero.

The source of each component of the fluctuation is well understood: The initial negative transient is due to the transition $x_6 \rightarrow x_0$ of the secondary activation kinetics because of the direct voltage-dependence of its rate constants (Fohlmeister and Adelman, 1985*b*, Eq. 7a, b). Simultaneously, but on a slower time scale, the primary activation kinetics make transitions from substate x_5 to x_4 and lower states that also contribute a (smaller) negative current component. The positive component of the fluctuation is due to the return transitions $x_0 \rightarrow x_6$ of the secondary kinetics responding to the population shift in the primary mechanism. Transitions of the primary kinetics subsequently dominate the (negative) gating current for the remainder of the transient.

Having presented this description, we must add that it is unlikely that these fluctuations will be observed even with a voltage-clamp system of sufficient temporal resolution: Note that the fluctuation is due entirely to the direct voltage-dependence of the secondary kinetic transitions, and is fully over within the first 100 μs of the OFF step, which corresponds to frequency components >10 kHz. Although we have no data for $f > 5$ kHz, the results in Fohlmeister and Adelman, (1985*b*) show that the direct voltage-dependence of the rate constants of the secondary activation kinetics decreases with increasing frequency, and is already near zero at 3 kHz. Because the entire fluctuation is due to an imposed but unrealistic voltage-dependence (for $f = 500$ Hz) onto the secondary rate constants, we would predict that those fluctuations will not appear in transient gating current records. In simulations of the OFF response with voltage independent secondary rate constants, the current shows a monotonic decline after an instantaneous (no rising phase) onset (see Fig. 10, solid curve).

The weakening of the voltage-dependence of the secondary process rate constants does not imply a weakening in the coupling between the primary and secondary activation processes; that coupling is a local phenomenon within the molecule and the rate constants of the secondary process will remain relatively large (see Eqs. 7a, b in Fohlmeister and Adelman, 1985*b*). Based on the data in Fohlmeister and Adelman (1985*a*), the secondary activation process therefore has the following properties: (*a*) Secondary kinetic transitions respond to the local field change due to a primary kinetic transition to, or from substate x_5 with a mean time delay of ~5 μs (k_{06}, $k_{60} \sim 200$ ms^{-1}). (*b*) Secondary kinetic transitions respond directly to changes in the average transmembrane field with a time delay of ~0.15 ms. This estimate is based on the rate of weakening of the direct voltage-dependence of the secondary process rate constants with increasing command frequency. (*c*) The occurrence of a kinetic transition of the secondary process is registered as gating current with no (or negligible) time delay. An upper limit on the latter time delay is given by the inherent response times of the voltage-clamp system.

A Hypothetical Molecular Model

In the analysis of the present data, reciprocal steric hindrance has been the principal hypothesis for both the coupling between activation and inactivation, and the mechanism for the control of inactivation gating. It is therefore necessary for us to demonstrate how this mechanism could be envisioned in molecular detail. In the absence of the detailed primary amino acid residue sequence for the Na-channel protein for *Loligo pealei* we base our model structure on the sequence for *Electrophorus electricus* (Noda et al., 1984). Although the primary sequence for the two species may differ in detail, we assume that the tertiary structures are functionally similar. The entire gating machinery to be described is situated on the axoplasmic side of the membrane. Fig. 7 of Fohlmeister and Adelman (1985*b*) gives segments of the secondary structure of the sodium-channel protein (Noda et al., 1984, Fig. 6*B*) that are folded to yield a hypothetical channel (Figure 13 *A*) and activation gate. The tepee structure, that forms a closed model activation gate (Fig. 13 *D*), and whose conformational changes are associated with the secondary activation kinetics, is anchored on the channel rim on the axoplasmic side of each of the four similar (homologous) protein domains that are suggested by the primary sequence (Noda et al., 1984). The anchor points are so spaced as to provide room for four additional polypeptide chains to interdigitate between them (Figs. 13 *B* and *C*). Indeed, given the model channel of Fig. 13 *A*, the presence of these interdigitating elements is predetermined as the continuation of the primary residue sequence extending from the segments S1 (Noda et al., 1984, Figure 6 *B*) of each of the four homologous protein domains at the channel rim on the axoplasmic side. These interdigitating elements are hypothesized to be the inactivation gate. The elements correspond to the latter portion of amino acid residue sequences numbered 1–114, 403–557, 956–991, and 1,265–1,313, which lead directly into the onset of segments S1 given by residue numbers 115, 558, 992, and 1,314 (Noda et al., 1984, Fig. 3) The four inactivation segments are envisioned to lie in a plane parallel to the plane of the membrane near the axoplasmic surface, and extending outwards from the channel in four directions (Fig. 13 *B* and *C*). The directions are each orthogonal to the direction of its two neighbors, but the extended longitudinal axes of the elements are each slightly offset from the center of the channel opening so that no two arms have a common axis. These

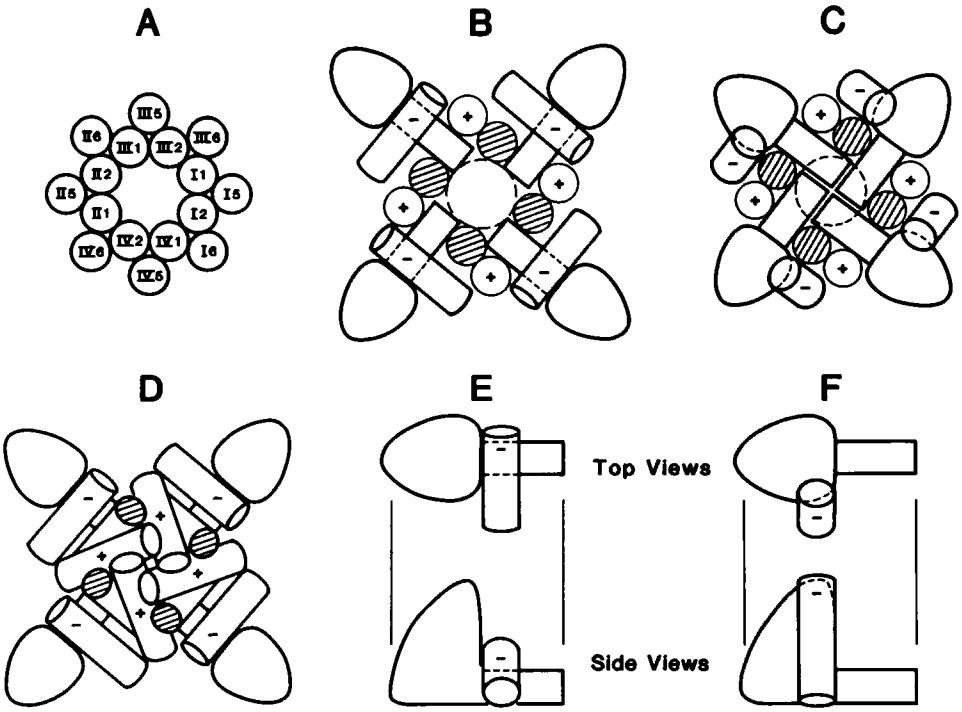

FIGURE 13 (*A*) Hypothetical arrangement of transmembrane α-helical segments given in Noda et al. (1984) to form a channel as viewed face on to the axoplasmic side of the membrane. Roman numerals identify each of four homologous subunits, and Arabic numerals identify segments within each homologous domain (Noda et al., 1984). (*B*) Hypothetical arrangement of inactivation elements (shafts with distal-end bulbous structures) in the non-inactivated position. The partially overlaying cylindrical structures (identified by a minus (−) sign) are associated with the primary activation gating kinetics. The four crosshatched circles, and the four circles containing a plus (+) sign represent α-helical segments S3 and S4, respectively, as identified in Noda et al. (1984). These eight segments are associated with the secondary activation kinetics, are viewed end-on, and correspond to an open activation gate. The channel is therefore in one of the allowed, but rarely occurring conducting conformations that corresponds to state $X_{1,0,0}$. (*C*) Hypothetical arrangement of inactivation elements in the inactivated position, blocking the channel opening. The primary activation gating elements (−) are in substate x_4, and are sterically prevented from lowering and entering substates x_3, x_2, or x_1. Secondary activation gating elements are as in *B*, and the channel is in the nonconducting conformational state $X_{4,0,1}$. (*D*) Gating protein elements in positions with the activation gate closed and the channel non-inactivated, corresponding to the resting state conformation $X_{2,6,0}$. (*E* and *F*) Top and side views of an individual inactivation protein element and a primary activation gating element corresponding to configurations *B* and *C*, respectively. Note the reciprocal steric constraints between the inactivation and primary activation elements imposed by the hypothetical structures and positions of the elements.

elements are postulated to lie beneath, and extend laterally beyond the protein elements that are associated with the primary activation gating mechanism (cylinders identified by a minus (−) sign in Fig. 13). The distal ends of the inactivation elements are postulated to fold into secondary protein structures (possibly of a random coil nature) that substantially increase the physical bulk of those (end) portions of the four arms.

The dynamics of conformational change associated with inactivation gating depends on the substate that is occupied by the primary activation process. Consider first the case where molecule is in substate x_4 or x_5. Structurally, this corresponds to the protein elements of the primary process elevated, or extended away from the channel towards the axoplasm (Figure 13 *C*, and Fohlmeister and Adelman, 1985*b*, Fig. 7 *C*). This position gives free rein to the bistable inactivation system to make transitions between its substates h_0 and h_1, which are postulated to be movements in a direction that is along the longitudinal axis of each inactivation element. One direction ($h_0 \rightarrow h_1$) brings the element into closer proximity with the center of the channel opening (Fig. 13 *C*), and the reverse direction ($h_1 \rightarrow h_0$) fully removes the element from the channel opening (Fig. 13 *B*). An element in the proximal position (substate h_1) will overlap the channel opening sufficiently to block the transmission of Na-ions through the channel, thereby inactivating the channel. This hypothetical channel blockade is facilitated by the fact that two of the innermost three amino acid residues are positively charged on three of the four postulated arms (the positive residues are numbered 113, 114, 556, 557, 990, and 991; Noda et al., 1984, Fig. 3).

Given the rate constants, $K_{01} = 2.0\ \text{ms}^{-1}$ and $K_{10} = 0.125\ \text{ms}^{-1}$ (Eq. 4), the channel will spend most of its time in the inactivated state h_1, the equilibrium constant being $K_{01}/K_{10} = 16$. During the relatively long time intervals that an arm is situated in the inactivated substate h_1, the distal, bulky end of the arm is positioned beneath the primary activation protein element, thereby preventing that element from lowering, and entering substate x_3, by steric hindrance (Fig. 13 *C* and *F*). The effect is to substantially reduce the amplitude of the gating current that would otherwise be generated by the primary activation gating process as a result of kinetic transitions to, and among substates x_3, x_2, and x_1 for noninactivated channels.

Although a channel will spend most of its time in substate h_1 when the primary activation mechanism occupies substates x_4 or x_5, it will, on a time scale of 8 ms, enter substate h_0. During the time intervals that the channel occupies substate h_0 it becomes possible for the protein elements associated with the primary activation mechanism to lower (towards the center of the membrane) and enter substates x_3, x_2, and x_1 because the inactivation element is now in its distal position relative to the channel opening, with the bulky part of that element sufficiently far removed so as not to interfere with the movement of the primary activation mechanism (Fig. 13 *B* and *E*). Thus, steric hindrance on the primary process is relieved. Indeed, in this model of gating, the role of steric hinderer is now

exchanged, and the protein element of the primary activation process in substate x_1, x_2, or x_3 now blocks the transition to inactivation. This blockage occurs because the primary activation element in substate x_1, x_2, or x_3 is occupying the space that would otherwise be occupied by the bulky portion of the inactivation element when that element is in substate h_1 (Figs. 13 *E* and *F*).

Because the model channel molecule favors the inactivated substate, h_1, over substate h_0 when not sterically restricted by the primary activation element, the dominant forces that induce movement of the inactivation elements must be centrally directed (towards the channel opening). To be consistent with all experimental details, those forces (possibly applied by the polar head groups of neighboring lipid) must be applied on the distal, bulky end of the inactivation elements, which are the most exposed parts of the channel protein, and therefore also most susceptible to the action of enzymes. With that portion cleaved by protease, the driving forces toward inactivation can no longer be applied, and the channel will remain non-inactivated. The action of *N*-bromo-acetimide and other substances (c.f. French and Horn, 1984) that prevent inactivation, but are not peptides, might then be explained as being due to an interference with the dominant inactivation driving forces. This interference could also take the form of a steric blockade by the substance on the exposed bulky end of the inactivation elements.

The tertiary structures of the model sodium channel given in Fig. 13 contain 16 α-helical segments that span the hydrophobic (lipid) portion of the membrane, with eight of these segments lining the Na-ion pathway (Fig. 13 *A*). The lining segments are all amphipathic in the sense that charged residues appear on only one side of the helices with more than half of the circumference of each helix cylinder being strictly uncharged (except the segment identified as III1, for which 43% of the circumference contains no charges along its length). All charged residues are postulated to face the channel pore. The segments are identified by a roman numeral I to IV that gives the number of the homologous protein domain as specified in Nota et al. (1984), and by an Arabic numeral 1, 2, 5, or 6 that identifies the segment within each homologous domain (Noda et al., 1984). (All 8 segments 5 and 6 are uncharged and hydrophobic.) The particular order of the channel lining segments given in Fig. 13 *A* was chosen on the basis of charge location, which allows a maximum of salt bridges to be formed between neighboring segments for structural considerations. This arrangement also eliminates all positive charges from the channel lining (except at the pore opening on the axoplasmic side). However, the number of potential salt bridges is insufficient for a unique determination of the order of the channel lining segments. Nevertheless, discounting those charges that are assumed to be neutralized in salt bridges, there remains an orderly progression of negative charges throughout the channel. Assuming an axial distance of 1.5 Å per amino acid for each α-helix, the lipid spanning segments are 38–45 Å in length. Beginning at the periaxonal end, the first negative charge (residue #1020) appears near the channel opening on segment III1. In addition to this charge there is a net excess of 20 negative charges on the portion of the channel protein that protrudes on the periaxonal side and is not counted as part of the identified segments. This excess might be expected to concentrate dissolved sodium ions near the channel. The second negative charge (residue #1035) appears at ~7.5 Å into the channel on segment III2. The third charge (residue #152) appears at ~13.5 Å on segment I2. Beyond this point there appear to be two strong sites consisting of 3 negative charges each. The first occurs at ~25.5 Å consisting of residues 569, 1,003, and 1,325 on segments II1, III1, and IV1, respectively. The second occurs at ~30 Å consisting of residues 162, 565, and 1000 on segments I2, II1, and III1, respectively. The final negative charge (residue #1317) appears at ~37.5 Å on segment IV1. We have not determined any particular function for the two neighboring and deep potential wells near the center of the model channel (this may be a location where transient Na ions can pass each other within the channel), but consider their presence, and the systematic order of sites along the channel as constituting a reasonable potential energy profile for a monovalent cation selective pathway. This assessment is based on the fact that the spacing of negative charges throughout the model channel corresponds very closely to the average spacing of (negative) counterions in an aqueous solution of 0.3–1-M concentration.

Received for publication 18 December 1985 and in final form 11 March 1986.

REFERENCES

1. Armstrong, C. M., and F. Bezanilla. 1977. Inactivation of the sodium channel II: gating current experiments. *J. Gen. Physiol.* 70:567–590.
2. Armstrong, C. M., and W. F. Gilly. 1979. Fast and slow steps in the activation of sodium channels. *J. Gen. Physiol.* 74:691–711.
3. Bezanilla, F., and C. M. Armstrong. 1977. Inactivation of the sodium channel I: sodium current experiments. *J. Gen. Physiol.* 70:549–566.
4. Bezanilla, F., M. M. White, and R. E. Taylor. 1982. Gating currents associated with potassium channel. *Nature (Lond.).* 296:657–659.
5. Fishman, H. M., L. E. Moore, and D. Poussart. 1977. Asymmetry currents and admittance in squid axons. *Biophys. J.* 19:177–183.
6. Fohlmeister, J. F., and W. J. Adelman. 1985*a*. Gating current harmonics I: sodium channel activation gating in dynamic steady states. *Biophys. J.* 48:375–390.
7. Fohlmeister, J. F., and W. J. Aldeman. 1985*b*. Gating current harmonics II: model simulations of axonal gating currents. *Biophys. J.* 48:391–400.
8. French, R. J., and R. Horn. 1983. Sodium channel gating: models, mimics and modifiers. *Annu. Rev. Biophys. Bioeng.* 12:319–356.
9. Gilly, W. F., and C. M. Armstrong. 1980. Gating current and potassium channels in the giant axon of the squid. *Biophys. J.* 29:485–492.
10. Hodgkin, A. L., and A. F. Huxley. 1952. A quantitative description of membrane current and its application to conduction and excitation in nerve. *J. Physiol. (Lond.).* 117:500–544.
11. Noda, M., S. Shimizu, T. Tanabe, T. Takai, T. Kayano, T. Ikeda, H. Takahashi, H. Nakayama, Y. Kanaoka, N. Minamino, K. Kangawa, H. Matsuo, M. A. Raftery, T. Hirose, S. Inayama, H. Hayashida, T. Miyata, and S. Numa. 1984. Primary structure of *Electrophorus electricus* sodium channel deduced from cDNA sequence. *Nature (Lond.).* 312:121–127.
12. Takashima, S. 1978. Frequency domain analysis of asymmetry current in squid axon membrane. *Biophys. J.* 22:115–119.
13. Taylor, R. E., and F. Bezanilla. 1979. Comments on the measurement of gating currents in the frequency domain. *Biophys. J.* 26:338–340